Bayesian approach for auroral oval reconstruction from ground-based observations

D. Wagner[1], R. Neuhäuser[1], R. Arlt[2]

[1]Astrophysikalisches Institut und Universitäts-Sternwarte Jena, Schillergässchen 2, 07745 Jena, Germany

[2]Leibniz Institute for Astrophysics Potsdam, An der Sternwarte 16, 14482 Potsdam, Germany

Key Points:

- The position and size of the auroral oval can be reconstructed by using ground-based observations
- Synthetic observations were used to validate the method
- The results for four modern geomagnetic storms are in good agreement with the measurements

Corresponding author: D. Wagner, wagner.d@uni-jena.de

Abstract

To understand long term variability of solar activity, homogeneous time series are required. However, proxies like the Zurich sunspot number or cosmogenic isotopes suffer from discontinuities. Naked eye observations of aurorae, however, might be used to bridge discontinuities in solar activity indices in order to approach a homogeneous solar activity record. With information derived from aurora observations like observing site, time of aurora sighting and position on sky we can reconstruct the auroral oval. Since aurorae are correlated with geomagnetic indices like the Kp index, it is possible to obtain information about the terrestrial magnetic field in the form of the position of the magnetic poles as well as the magnetic disturbance level.

Here we present a Bayesian approach to reconstruct the auroral oval from ground-based observations by using two different auroral oval models. With this method we can estimate the position of the magnetic poles in corrected geomagnetic coordinates as well as the Kp index. The method is first validated on synthetic observations before it is applied to four modern geomagnetic storms between 2003 and 2017 where ground-based reports and photographs were used to obtain the necessary information. We have shown that we are able the reconstruct the pole location with an accuracy of $\approx 2^\circ$ in latitude and $\approx 11^\circ$ in longitude. The Kp index can be inferred with a precision of one class.

The future goal is to employ the method to historical observations.

1 Introduction

Aurorae occur in oval like zones around the geomagnetic poles as was first noticed by *Feldstein* [1964] after analysis of all-sky camera images. Due to the interaction of the earth's magnetosphere with the interplanetary magnetic field carried by the solar wind the oval has complex shape. There are several models describing the position, size and shape of the auroral oval and linking it to different parameters, like solar wind parameters in the case of the Ovation Prime Model [*Newell et al.*, 2009], which is mostly used for aurora forecasting. Other models connect the oval size to the level of geomagnetic disturbance described by the Kp index [e.g. *Holzworth et al.*, 1975; *Zhang and Paxton*, 2008]. The Kp index is a 3-hour index derived as the mean value of the Ks indices of 13 magnetic observatories describing the global level of geomagnetic disturbance on a quasi-logarithmic scale [*Bartels et al.*, 1939]. Since the magnetic indizes like the Kp index or the closely related aa index also show the solar cycle [*Sabine*, 1852], they can be used to study present

and past solar activity. *Siscoe and Verosub* [1983] pointed out that in case of 100 % accurate observations of all aurorae it would be possible to derive the temporal evolution of the solar activity and the position of the geomagnetic pole. Until now, solar activity derived from aurora sightings is only based on aurora frequency, meaning that aurorae are more likely to occur in phases of high solar activity (*Neuhäuser and Neuhäuser* [2015a], *Neuhäuser and Neuhäuser* [2015b], *Bekli and Chadou* [2019]). In this work, we present a method to reconstruct the position and size of the auroral oval from ground-based observations. The extent of the oval provides the Kp index, whence information about solar activity. This is in particular of interest for pre-instrumental times, where reconstructing the auroral oval from ground-based observations yield information about the position of the geomagnetic pole as well as the magnetic activity.

Siscoe and Verosub [1983] narrowed down statistically the longitude of the geomagnetic pole by using the auroral frequency in Japan and China between the 800 and 1400 A.D. Again, only the auroral frequency is used, in contrast to the reconstruction of the oval, which is the aim of this work. *Korte et al.* [2016] used a circular approximation of the auroral oval together with reconstructions of solar activity and the Earth's magnetic field to limit the range of possible aurora sightings in the last millennia. A comparison with known observations provided a good agreement. Unlike the model of *Korte et al.* [2016], neither the Kp index nor the position of the pole is predefined in the present work. Furthermore, models of the geometry of the oval are used instead of a circular approximation, which, depending on the magnetic local time, yields differences in the auroral oval latitude of $\sim 10^{\circ}$.

The main goal of this work is to develop a method to reconstruct the auroral oval from ground-based aurora sightings for eventual use with historical data, which also delivers the Kp index providing information about solar activity. This information can be used for comparison with other reconstructions of solar activity, for example from sunspot numbers [*Clette et al.*, 2014] or cosmogenic isotopes like ^{14}C and ^{10}Be [*Usoskin*, 2017]. An independent activity measure from aurorae may be helpful in understanding inhomogeneities in the sunspot or isotope records.

The position of the magnetic pole is reconstructed from the position of the oval and can be compared with the results from different paleomagnetic field models as described in *Korte et al.* [2018].

This paper is structured as follows: Section 2 briefly discusses Bayesian inference, introduces the auroral oval models from *Holzworth et al.* [1975] and *Zhang and Paxton* [2008] used here and describes the implementation. The method is first tested on synthetic observations before it is applied to four modern geomagnetic storms between 2003 and 2017 in Section 3. There we also explain how ground-based observations in form of photographs and reports are utilized to obtain all the necessary information to successfully apply the developed method. In Section 4 we summarize our findings and give a short outlook.

The method and results described in this paper are based on the PhD thesis by *Wagner* [2020].

2 Bayesian method for auroral oval reconstruction

We use Bayesian inference for reconstructing the auroral oval from ground-based observations employing either of two auroral oval models. The free parameters which are inferred are the coordinates of the pole in corrected geomagnetic (cgm) coordinates and the Kp index. A posterior probability density distribution is calculated from which we can obtain confidence intervals for the desired parameters. Bayesian statistics describes the probability of a model under the given data, in contrast to classical statistics where the probability of the data is calculated under a given model.

The method is first tested on synthetic observations for which the parameters are known. Afterwards we apply the method to four modern geomagnetic storms between 2003 and 2017.

2.1 Bayesian inference

Bayesian inference is based on Bayes' theorem [*Bayes*, 1764; *D'Agostini*, 2003], stating that the probability of obtaining certain data given external circumstances (the "mode") can be converted into a probability of certain circumstances given the data. Hence, we calculate the likelihood of a parameter set of an auroral oval given the data obtained from reports and photographs of the aurora. The parameter estimation (latitude and longitude of the cgm pole as well as Kp index) is then based on the posterior distribution over the whole parameter space which provides directly the confidence intervals. Monte Carlo Markov Chains (MCMC) are used, which are algorithms sampling a probability distribu-

tion and converging to the posterior distribution [*Robert*, 2016] without actual integration. The Metropolis-Hastings formalism used here was first described by *Hastings* [1970]. Dependent on the current position of the Markov Chain a new value in the proximity is proposed. If the new value has a higher probability, it usually is accepted. With a certain probability, however, the old value is maintained. This ensures that the Markov chain is not limited to a local maximum. The distributions of the individual parameters is obtained by marginalisation over the other parameters (see appendix A: Figure A.2).

The code performing the Bayesian inference is based on the implementation by *Fröhlich et al.* [2012] and *Corsaro et al.* [2013] and is directly derived from *Arlt et al.* [2013] who inferred sunspot positions from historical observations.

2.2 Models of the auroral oval

The theoretical description which contains the free parameters of interest involves a model linking the Kp index to the oval size. First we use the model presented in *Holzworth et al.* [1975], which was later connected to the Kp index by *Starkov* [1994]. The second model was developed by *Zhang and Paxton* [2008]. Both use three input parameters, the latitude and longitude of the cgm pole and the Kp index. The oval expansion from both models increases linearly with Kp as shown by *Wagner and Neuhäuser* [2019].

Since, the model of the auroral oval presented in *Holzworth et al.* [1975] was developed using ground-based all-sky camera images, it is expected that the oval boundaries are consistent with naked-eye ground-based observations. It uses a circular approximation of the auroral oval boundaries with an additional Fourier component [*Korte et al.*, 2016]. As shown in *Holzworth et al.* [1975] the AL index is calculated from the Kp index with a set of coefficients. The latitude of the auroral oval boundaries is then obtained from a Fourier series in an amplitude-phase form, were again several coefficients are required. These coefficients are given in the work from *Holzworth et al.* [1975] as well as *Starkov* [1994] and *Sigernes et al.* [2011].

The second model used in this paper was developed by *Zhang and Paxton* [2008] and is based on UV images taken with the Global Ultraviolet Imager (GUVI) onbord the Thermosphere Ionosphere Mesosphere Energetics and Dynamics satellite (TIMED). Observational data from 2002 to 2005 led to an empirical model (hereafter ZP model), which describes the electron energy flux Q [ergs/s/cm^2] of precipitating electrons. The boundaries of the oval are defined as the locations where the electron energy flux is 0.25 ergs/s/cm^2.

Again, the position of the cgm pole and the Kp index are free parameters. Since this model is based on UV satellite data caution is due here, as the boundaries may not coincide with the aurora positions observed from the ground. *Kosar et al.* [2018] compared ground-based amateur observations of the aurora with the equatorward boundary of the ZP model at 0.2 ergs/s/cm^2 and found a 1-σ agreement with observations from the ground. The definition of a different boundary flux of 0.05 ergs/s/cm^2 has very little effect on the geographical position of the boundary ($\sim$ 0.5°). *Sigernes et al.* [2011] examined the extent to which both models agree with each other. They found that the agreement decreases with increasing Kp, whereby the ZP model describes a larger oval than the model presented in *Holzworth et al.* [1975]. It should be mentioned that both models are less accurate for large magnetic activity, since high activity occurs much less frequently and therefore the data available in these cases is limited. Nevertheless both models are applied to moderate as well as strong geomagnetic storm, because only such storms provide a sufficient number of observations for auroral reconstruction.

Both models describe the position of the poleward and equatorward boundary in corrected geomagnetic coordinates. Since the ground-based observations are given in geographical coordinates a transformation of the boundary positions is necessary. In order to calculate geographical from cgm coordinates, the tracing of field lines is necessary [*Laundal et al.*, 2017]. The cgm coordinates of any point P_0 are calculated by tracing the field line, according to a geomagnetic reference field, intersecting the point P_0 to the equatorial plane of the geomagnetic coordinates. To find the latitude ϑ_{cgm} in cgm coordinates, one earth radius $\mathrm{R_E}$ is used as a reference, $\vartheta_{\mathrm{cgm}} = \pm \arccos \sqrt{R_{\mathrm{E}}/(R_{\mathrm{E}} + h_{\mathrm{eq}})}$, where $\mathrm{h_{eq}}$ is the height at which the field line intersects the equatorial plane of the geomagnetic coordinates. The longitude ϕ_{cgm} is the longitude of the intersection. Thus, for correct conversion between cgm and geographic coordinates in which the observational data is given, a magnetic field model, which indicates the position and shape of the field lines, is required. However, the aim of this work is to actually determine the position of the cgm pole. Using a field model would already predefine the position of the cgm pole, which would contradict the goal. Furthermore, the method shall be extended to historical geomagnetic storms for which no sufficiently accurate reference field model (analogous to the International Geomagnetic Reference Field (IGRF-12) [*Thebault et al.*, 2015]) is available. Therefore, in the context of this work a restriction to the transformation given in *Sigernes*

et al. [2011] is necessary. Here it is assumed that the models use the cgm pole as reference point, but a simple rotation of the coordinate system from the cgm pole at longitude ϕ_0 and co-latitude Θ_o towards the geographic pole is performed. The cgm positions of the oval boundary from any of the models are converted into the geographical longitudes and latitudes, ϕ_g and ϑ_g.

2.3 Calculation of the auroral oval and the elevation of the aurora

For any geographical location and moment in time, any presumed Kp index and position of the cgm pole, we need to compute the theoretically expected elevation of the aurora above the horizon. Each set of model parameters is evaluated by comparing the theoretical elevation angle α' with the observed elevation angle α, which is given in aurora photographs or reports. First, we compute the boundary of the auroral oval. Only the equatorward boundary of the oval is used, since observers at mid-latitudes are more likely to see and report this boundary.

In detail, we determine the theoretical elevation angle α' for an altitude of $h = 500\,\text{km}$ [*Akasofu*, 2009]), since observers in mid- and low-latitudes most likely witness this part of the auroral oval. However, the lowest part of the aurora is at an altitude of around 100 km [*Akasofu*, 2009], so a different altitude might effect our results. With Equation 7 we determine the difference between the observer and aurora location. Changing the altitude of the aurora between 100 km and 500 km results in a similar variation as keeping the altitude fixed and changing the elevation angle in a $\pm 10°$ interval as performed in Section 2.5. Since there are no significant differences in the results with and without an additional variation of the auroral elevation angle (see Section 2.5), we conclude that changing the altitude within the aforementioned interval will have no significant effects on our results. If the determined position of the equatorward boundary is south of the observation site (in the northern hemisphere), it is assumed that the theoretical elevation angle is $\alpha' = 90°$. An observer in this scenario would be located within the auroral oval and observations should have been possible in the zenith. If we do not implement this assumption the theoretical elevation angle would again be in an interval between 0° and 90°. However, since the oval boundary is now closer to the equator than the observer this would indicate an observation in southern direction on the northern hemisphere. The code in this case is not able to distinguish between an observation to the north and south, though. This will be implemented in further steps. We do not expect any significant ef-

fects on our results in a $\pm 10^\circ$ interval for the elevation angle. For the Holzworth model we do not see any differences in the results of the four investigated geomagnetic storms when implementing this assumption. Since the oval described by this model is much smaller than the oval from the ZP model, none of the observations is within the equatorward boundary. When using the ZP model, however, the code fails to produce consistent results if the assumption is not taken into account. In our method only a single point on the oval is calculated, which leads to a drastic minimization of the calculation time. The magnetic local time (MLT) must first be calculated taking into account the geographical position of the cgm pole, the position of the observer and the local time of the observation. For this purpose the observation location is converted into corrected geomagnetic latitude and longitude using the corresponding inverse spherical transformation. The MLT is then calculated through

$$\mathrm{MLT} = \mathrm{LT} + \frac{(\phi_0 + \phi_{mB} - \phi_B) \cdot 24}{360^\circ}, \tag{1}$$

where ϕ_{mB} and ϕ_B are the magnetic and geographic longitudes of the observer. The second term in Equation 1 describes the time difference between the geographical and cgm system, which is added to the local time LT of the observer. Our free parameters are again needed here in terms of the geographical longitude ϕ_0. This means for each iteration of the parameters, the MLT is part of the theoretical description and not a property of the observation.

The final theoretical elevation α' is obtained through the geocentric angle

$$d = \arccos[\sin(\vartheta_{\mathrm{Oval}})\sin(\vartheta_{\mathrm{B}}) + \cos(\vartheta_{\mathrm{Oval}})\cos(\vartheta_{\mathrm{B}})\cos(\phi_{\mathrm{B}} - \phi_{\mathrm{Oval}})]. \tag{2}$$

between the point ($\vartheta_{\mathrm{Oval}}$, ϕ_{Oval}) on the aurora oval and the position of the observer (ϑ_{B}, ϕ_{B}). This means that an observer looking in magnetic north direction sees this point of the aurora oval (see Figure 1), where point 1 describes the location of the equatorward boundary of the oval. Note that we speak of "magnetic north direction" for the magnetic pole in the northern hemisphere in order to avoid confusion. If an observer looks in a direction DIR other than north, point 2 is seen for example.

The theoretical elevation angle α' follows from

$$\alpha' = \arctan\left(\frac{\cos(d) - \frac{R_{\mathrm{E}}}{R_{\mathrm{E}}+h}}{\sin(d)}\right), \tag{3}$$

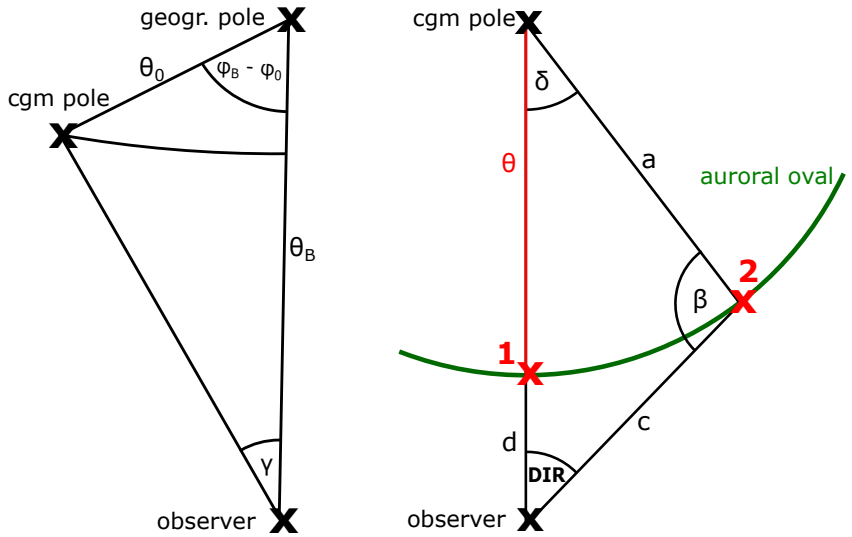

Figure 1. Left: Relations for converting between geographical and cgm cardinal direction. The difference in geographical longitude between observer and cgm pole is described with $\phi_B - \phi_0$. The co-latitude of the cgm pole and the observer is described with Θ_0 and Θ_B, respectively. The angle γ is sought. Right: The equatorward boundary is shown in green, simplified as a circle at the corrected geomagnetic co-latitude. In addition, an observing site and the cgm pole are shown. In the magnetic north direction, an observer sees point 1 of the oval which has the same MLT as the observer and which is the closest oval point to the observer at distance d. In a different direction DIR, point 2 of the oval is seen, which is further away from the observer than point 1.

where h is the height above sea level of the upper limit of the aurora curtain ($h = 500\,\mathrm{km}$). For observations in magnetic north direction the theoretical elevation angle of the aurora can be calculated immediately.

If the observation took place in another direction, given by the azimuth of the aurora, the distance c in Figure 1 needs to be determined. In addition, the information about the cardinal direction given in reports uses the geographical system as reference. Therefore, an additional conversion of the geographical direction into the magnetic direction (DIR) is necessary. Again knowledge about the position of the cgm pole is required, which is a free parameter within the program. The conversion of the cardinal direction in both systems is done by geometrical relations of the spherical triangle shown in Figure 1 on the left side, consisting of the geographic pole, the cgm pole and the observer. The spherical triangle has been simplified for illustration purposes. We are looking for the angle γ, which indicates the difference between the cardinal direction in the geographical and cgm

system. Using angular relationships in spherical triangles we get

$$\gamma = \arcsin\left[\frac{\sin\Theta_0 \cdot \sin(\phi_B - \phi_0)}{\sin[\arccos(\cos\Theta_B \cdot \cos\Theta_0 + \sin\Theta_B \cdot \sin\Theta_0 \cdot \cos(\phi_B - \phi_0))]}\right], \tag{4}$$

where Θ_B is the geographic co-latitudes of the observer. Addition of γ with the given cardinal direction in geographic coordinates yields the magnetic cardinal direction DIR. Once DIR is known, the distance c can be calculated. To make this possible, the aurora oval, as shown in Figure 1 right, must be locally assumed to be circular (so $a = \Theta$). Otherwise, the MLT of the place of the oval where the observer sees the aurora would be required. However, it is impossible to determine this MLT with the given information, because in the irregular triangle consisting of observer position, cgm pole and point 2 in Figure 1 right only the angle DIR and the adjacent distance $\Theta + d$ are known. It is nevertheless useful to use the above mentioned models of the auroral oval, because they give the correct co-latitude in magnetic north direction, which is dependent on the local time due to the complex shape of the auroral oval. If the entire oval were approximated with a circle, this dependence would be eliminated. The law of sines first delivers the angle $\beta = \pi - \arcsin[\sin(\Theta + d)\sin\mathrm{DIR}/\sin\Theta]$. Then c can be calculated using the Napierian equations.

$$c = 2\arctan\left[\frac{\tan\left(\frac{2\theta+d}{2}\right)\cos\left(\frac{DIR+\beta}{2}\right)}{\cos\left(\frac{DIR-\beta}{2}\right)}\right]. \tag{5}$$

The elevation α' can now be calculated using (3) where c replaces d. The difference between the theoretical elevation angle and the observed elevation angle $(\alpha - \alpha')$ is our test quantity for the model parameters.

The elevation angle given in the observations is subject to measurement uncertainties. The model with its parameters has a likelihood Λ to have created the data set, which is the product of all likelihoods to have created individual data points. Since we are dealing with observational uncertainties, the likelihood is not a sharp function, but a distribution defined by a measurement variance σ^2. The exact measurement uncertainties are extremely difficult to assess; we therefore use Gaussian distributions for practical reasons. The likelihood given a set of parameters is then

$$\begin{aligned}\Lambda(\phi_0, \Theta_0, \mathrm{Kp}) &= \prod_{i=1}^{n}(2\pi\sigma^2)^{-\frac{1}{2}}\exp\left[-\frac{1}{2\sigma^2}\left(\alpha_i - \alpha_i'\right)^2\right] \\ &= (2\pi\sigma^2)^{-\frac{n}{2}}\exp\left[-\frac{1}{2\sigma^2}\sum_{i=1}^{n}\left(\alpha_i - \alpha_i'\right)^2\right],\end{aligned} \tag{6}$$

where the α_i' are functions of ϕ_0, Θ_0, and Kp and σ is assumed to be 10°. The latter value is estimated from the accuracy with which the elevation angle can be obtained from

the photographs. The values for the root mean square deviation calculated in Section 3.2 are in a similar range, meaning that a σ of 10° is a good estimate for the measurement uncertainties. The free parameters can be constrained. The longitude of the cgm pole ϕ_0 can have values between $-\pi$ and π. The latitude was limited to the interval between sin(50°) and sin(90°). The sine ensures a uniform distribution of random points on the sphere. The lower value is derived from the paleomagnetic field models discussed in [*Korte et al.*, 2018]. These suggest that the latitude of the geomagnetic pole has never been less than $\approx 76°$ over the last 10 000 years. However, in order not to limit the interval too much and to allow further freedoms, a latitude of 50° was chosen. The Kp index has a range from 0 and 9+ [*Bartels et al.*, 1939]. Since no further information about these parameters is known and since it is assumed that the pole is considered equally probable for all positions and that all Kp values are equally probable, an prior distribution in the form of a continuous uniform distribution is chosen which is restricted to an interval.

The full integration of the likelihood over three parameters is numerically challenging. Monte Carlo Markov chains (MCMC) are therefore used to explore the parameter space. Certain step parameters control the "wiggle room" of the Markov chains and are chosen in such a way that the parameter space is efficiently explored. A value of 0.1 in radians is assumed for the geographical longitude, 0.08 for the sine of the latitude, and 0.5 for the Kp index. If these sigmas are too large, the resulting probability density distributions are very broad and overestimate the confidence intervals; if they are too small, the parameter space may not be fully explored. The step values are means, while the actual implementation uses adaptive step values.

If the data quality or quantity is poor, we can reduce the freedom of the model by setting fixed values for the parameters, meaning that the position of the cgm pole can be fixed to determine the Kp index exclusively. Since 1900, the position of the cgm pole is available from the IGRF [*Thebault et al.*, 2015].

2.4 Limits of the method

For the method developed here, it is important that the auroral oval models can be used to determine a theoretical elevation angle of the aurora for each observation. In some cases, however, where the observer has looked in a direction very different from the

magnetic north, this is not possible. In these cases, according to the model, the observer should not have been able to see the aurora at this point. These cases are less frequent when using the model from *Zhang and Paxton* [2008] which describes a larger oval than the model from *Holzworth et al.* [1975]. Nevertheless, they may be an indication that both models underestimate the extent of the auroral oval for large Kp indices. It is likely that both models are fairly accurate when it comes to weak and moderate geomagnetic storm (see Section 3.3). As shown in *Wagner* [2020] the difference in both models becomes larger as the Kp index increases. For a Kp index of 9+ the difference in the maximum oval expansion is around 20°, indicating that the Holzworth model has an uncertainty of at least 20° for strong magnetic activity. Since even the ZP model underestimates the auroral oval size for extreme events, the error is probably even lager. For now we are limited to the possibility to alleviate the problem for instance by neglecting the given cardinal direction and to assume that the observation was made in magnetic north direction. This variant leads to a solution for all observations, but ignores known information. Alternatively, the observations for which there is no solution according to the model could be neglected, but this limits the amount of data. A compromise is to include the direction for all observations for which the models provide a solution and to assume magnetic north as direction only in the remaining cases. We have tried these three variants.

In a completely different approach, we do not compare theoretical and observed elevation angles, but use the physical distance of the observed aurora in the atmosphere to the nearest point on the theoretical oval to determine the likelihood of any parameter set. The aurora position is calculated based on the observational data in 3D Cartesian coordinates. The disadvantage is that we used derived quantities instead of observed ones, which violates the idea of Bayesian inference. We determine the position of the aurora from an observed elevation angle α and azimuth $\overline{az}$ through the geocentric angle g between the observer and the aurora can be determined by

$$g = 90^\circ - \alpha - \arcsin\left(\frac{R_\mathrm{E}}{R_\mathrm{E} + h} \cdot \cos(\alpha)\right). \tag{7}$$

The aurora was then observed approximately above the geographical position

$$\Delta\phi = g \cdot \sin(\overline{az}), \qquad \Delta\vartheta = g \cdot \cos(\overline{az}), \tag{8}$$

where $\Delta\phi$ and $\Delta\vartheta$ describe the differences in longitude and latitude to the observer's geographical position. Afterwards a conversion to 3D Cartesian coordinates is performed with the Matlab routine *ell2xyz* from the "Geodetic Toolbox Version 2.99.0.0" by Mike

Craymer[1] using WGS84 [*Deparment of Defense*, 1991]. The distance between the resulting position of the aurora and the vector (x_g, y_g, z_g) of the nearest oval position from the models determines the likelihood of any parameter set of the given model. By this procedure a solution can be generated for each observation, since an intersection with the actual oval is not necessary. Again, both oval models mentioned above can be used.

In total, there are now four different methods and two approaches available to reconstruct the auroral oval. Either the observed elevation angle is compared with the theoretical elevation angle calculated from the models (Approach A), or the 3D location of the aurora is calculated from the observations and is compared with the closest location of the aurora from the models (Approach B). The different approaches and methods are summarised in Table 1. All the different methods are applied to the investigated geomagnetic storms.

Table 1. Overview over the different methods and approaches. The grey-shaded methods use the model according to *Zhang and Paxton* [2008], whereas in the other cases the model according to *Holzworth et al.* [1975] is used. In addition, the two comparison approaches are given (A: elevation angle, B: atmospheric distance of the aurora). The third column describes whether the direction (azimuth) given in the reports/photographs has been included.

Nr.	Approach	Direction	Description
1	A	no	all observations in magnetic north direction
2	A	yes	if no solution in given direction → obs. in magnetic north
3	A	yes	ignore observations without solution
4	B	yes	calculate aurora position in Cartesian coordinates, compare with models
5	A	no	all observations in magnetic north direction
6	A	yes	if no solution in given direction → obs. in magnetic north
7	A	yes	ignore observations without solution
8	B	yes	calculate aurora position in Cartesian coordinates, compare with models

2.5 Testing the method on synthetic observations

Synthetic observations were created for which the Kp index and the position of the cgm pole is known. For this purpose random observing sites were generated in a prede-

[1] `https://de.mathworks.com/matlabcentral/fileexchange/15285-geodetic-toolbox`

fined geographical latitude range. We randomly assigned a time and an azimuthal direction, corresponding to the magnetic cardinal direction, to each auroral observation. In the case of the time, the interval was limited to 21:00 to 03:00 local time, whereas directions between −45° and 45° with respect to the magnetic north direction were allowed. Subsequently, the above mentioned models were used to assign an elevation angle to each "observation" representing the angle given in reports or photographs. The Kp index and the position of the pole were predefined. In the following example, 40 observations between 40° and 60° northern latitude were created. We used an uneven distribution in longitude to mimic the observating site distribution during actual geomagnetic storms. The corresponding elevation angles were generated once from the Holzworth and once from the ZP model. The Kp index for these observations is 6 and the cgm pole was located at a geographic position of 83.1° N and 84.0° W. As a result, the different methods should return the given parameters. Figure 2 shows the geographical positions of the synthetic observations (blue) and the given cgm pole (red).

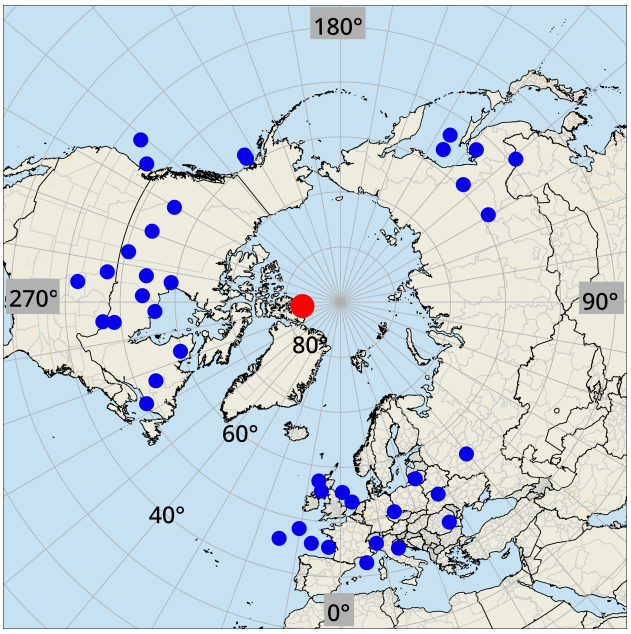

Figure 2. Geographical distribution of 40 synthetic observations (blue) as well as the position of the predefined cgm pole (red).

The derived parameters are consistent with the given values (see appendix A: Table A.1). Here method 2 is discussed more detailed. For the cgm pole, method 2 results in a geographical position of $(83.1 \pm 0.1)°$ N and $(84.1 \pm 3.5)°$ W. The obtained Kp index is

6.0 ± 0.4, so the calculated Kp index is given as a decimal number. The quasi-logarithmic scale of the Kp index can also be represented by decimal numbers. The minus behind the Kp value is equivalent to a reduction of the index by 0.33 (e.g. 6− = 5.67). The plus on the other hand describes an increase of 0.33 (e.g. 6+ = 6.33). Figure A.2 in appendix A: shows the probability distribution of all three parameters. A clear peak is visible in each case.

In order to simulate further inaccuracies in the observations, the calculated elevation angles of the synthetic sightings were randomly varied in a 10° interval around the previously determined value. We used a value of 10° since this is the typical uncertainty of the elevation angle obtained from the images. Again, results could be obtained which were in agreement with the specifications (method 2: cgm pole at $(83.2 \pm 0.1)°$ N and $(83.0 \pm 3.7)°$ W, Kp = 6.1 ± 0.5).

In the next step, the East Asian observations were neglected for the calculation, as sightings in East Asia are often missing in real storms. This left 34 synthetically generated observations in North America and Europe. We performed this step to check whether this has an effect on the result. The determined position of the cgm pole using method 2 is $(83.1 \pm 0.1)°$ N and $(84.2 \pm 3.6)°$ W. The calculated Kp index is 6.0 ± 0.5 The results do not change significantly and the given parameters can still be determined. Since the synthetic observations were generated using the models, the oval expansion is not underestimated in these cases, which is why consistent results were obtained even for high Kp indices. The results of the different methods using the Holzworth and ZP model are shown in appendix A: Table A.1. The table is structured analogously to Table 1. As mentioned above, all calculations were repeated with an additional variation of the elevation angle to check whether consistent results can be achieved even with larger deviations in the given elevation. An overview of these results can be found in appendix A: Table A.2.

While all methods reproduce the original values, it is noticeable that the longitude of the cgm pole has larger error ranges, when multiplied with cos(latitude), than the latitude. This behaviour is also shown later when investigating modern geomagnetic storms. Despite the larger error, the calculated value corresponds to the specifications. It becomes further clear that the methods with approach A and under consideration of the given direction (methods 2,3,6 and 7) deliver results which are closer to the original position, especially for the longitude of the cgm pole.

As a measure of the accuracy of the reconstructions, we compute the root mean square deviation (RMSD),

$$RMSD = \sqrt{\frac{1}{n}\sum_{i=1}^{n}(\alpha_i - \alpha_i')^2}, \tag{9}$$

where lower values mean better reconstructions. Methods 4 and 8 are based on a different approach and are therefore not comparable with the other methods, but only with each other. The RMSD values again show that the calculations give better results when the direction of the auroral display is taken into account. In addition, method 3 gives the lowest RMSD values. Here observations which do not deliver results according to the oval models are neglected, which is done by limiting the azimuthal interval, here from $-35°$ to $35°$. This resulted in the loss of six observations. The oval reconstructed with method 3 therefore reflects the observation data best. Methods 1 and 5, in which the direction of observation is not included, provide results that only agree with the specifications within $2\,\sigma$. The deviation is also reflected in a higher RMSD value. If possible, the directions of observation should therefore be included.

After neglecting the East Asian sightings, a similar picture emerges, with the RMSD values being somewhat higher overall. According to this, the reconstruction deteriorates with a more uneven global distribution, even if only minimally. In practice, this implies that auroral sightings with good global coverage should be sought if possible.

Similar to the Holzworth model, the Zhang Paxton model was tested using synthetic observations. It was found that, as before, the given parameters could be derived again. However, the calculated values usually only agree with the specifications within $2\,\sigma$. The RMSD values are in the same range as for the calculations using the Holzworth model, with method 7 (analogous to method 3 from the Holzworth model) again providing the best results. Since the synthetic observations were generated using the respective model, no estimation can be made here as to which model better reflects the distribution of observations. This comparison is only possible in the further course of the study on the basis of true observation distributions.

In appendix A: Table A.2 the results of the calculations after additional variation of the elevation angle within a $10°$ interval are shown. It can be seen that there is no significant change compared to the values shown in appendix A: Table A.1. Within the measurement uncertainties, the values are consistent with both the predefined values and the results without the additional variation. In addition, the RMSD values are also in the same order of magnitude and the developed methods provide good results even for larger un-

445 certainties in the observed elevation angle, but there are no significant differences in the
446 methods. We confirmed in all cases that the developed methods provide very good results
447 for artificially generated observations. In the next step, modern geomagnetic storms for
448 which the parameters are known from direct measurements, but the observations are real,
449 will be investigated.

450 3 Reconstruction of the auroral oval

451 To validate the developed methods for the reconstruction of the auroral oval, four
452 modern geomagnetic storms were used, for which the respective position of the cgm pole
453 and the Kp index are known with good accuracy, while the data are real observations. In
454 particular, amateur photographs of the auroras on the respective date were used to recon-
455 struct the auroral oval. We are limited to only a small number of modern geomagnetic
456 storms, since a sufficient number of observations is required in order to reconstruct the
457 oval. We mainly relied on the number of observations given in the aurora archive of An-
458 dreas Möller [*Möller*, 2021] and identified the four modern storms, which are discussed in
459 this chapter.

460 3.1 Data and data reduction

461 All-sky cameras are used to take aurora photos worldwide and provide elevation of
462 azimuth of the events. But cameras installed for other purposes can also yield informa-
463 tion. A good example is the all-sky camera of the university observatory of the Friedrich
464 Schiller University of Jena in Großschwabhausen monitoring weather conditions for as-
465 tronomical observations. Such cameras, as in this case on March 17, 2015, can also ran-
466 domly record northern lights.

467 In addition to professional data, amateur recordings are an important source of in-
468 formation. Databases are also available for such reports. For observations in Germany
469 and Central Europe the aurora archive of Andreas Möller was used [2]. The archive is con-
470 stantly updated and sightings are documented with reports as well as photos. In addition,
471 information on solar activity and geomagnetic activity for the respective storm is stored.
472 Another important archive is *Aurorasaurus* [*MacDonald et al.*, 2015], a citizen science
473 project where on-purpose and serendipitous aurora sightings can be reported. This data is

[2] http://www.polarlicht-archiv.de/

verified and made available online. In addition, Twitter posts are selected for certain keywords and checked for accuracy by users of the network. This constitutes a comprehensive database of aurora observations that can be used to improve forecasts and models.

In photographs, we determine the position of the aurora by using *Stellarium 0.16.1* [*Zotti et al.*, 2017] after identifying the background stars shown in the images (see appendix A: Figure A.1). If an aurora does not end at the edge of the image, the maximum extension shown was used. In cases where the aurora ends in certain areas of the image, the position at which the aurora can no longer be perceived is estimated. This is somewhat subjective, as it depends on the camera settings and also on the screen on which the photograph is viewed. To take this into account, sufficiently large error bars were assumed when reconstructing the oval (±10° for elevation and azimuth). For the following calculation the mean value of elevation and azimuth was used. The time of recording can also be constrained using *Stellarium* for photographs without details, using the background stars.

Figure A.1 in appendix A: shows an image of the Aurora Borealis in Hartenholm (53.900° N and 10.060° E) on March 17, 2015 at 23:30 LT. One can see the typical colours of the aurora, which change from green in the lower part to a red shade in the upper part. Also a slight ray-like structure, which is typical for active curtains, can be recognized. The lower panel of Figure A.1 shows the same section of the sky at the same location and local time in *Stellarium*. In the west, the aurora extends to the star β Tau, with an azimuth of 281°. In the east, the aurora ends near δ Her (AZ = 75°). The upper end of the auroral curtain can be seen in the area of Polaris, which has an elevation angle of 52°. Both the azimuth and elevation are then averaged to obtain the position which is later used in the calculation of the auroral oval.

3.2 Reconstruction of four geomagnetic storms

Here we present the results of the analysed storms. Table 2 gives an overview of important storm parameters: date, Kp index and position of the geomagnetic pole according to the IGRF-12 [*Thebault et al.*, 2015]. By using the *apexpy 1.0.1* code from Laundal and van der Meeren, which is based on a Fortran code from *Emmert et al.* [2010], we were able to determine the position of the cgm pole for the respective year. We calculated the Dst index from the geomagnetically equator-nearest aurora position [*Yokoyama et al.*, 1998] by using the following equation

$$\mathrm{Dst} \propto L_e^{-3}, \tag{10}$$

where L_e is related to the geomagnetic latitude ϑ of the equatorward boundary of the auroral oval via $L_e = 1/\cos^2 \vartheta$ and L_e is the geomagnetic latitude of the electron precipitation boundary. The geomagnetically equator-nearest auroral position for a given storm can thus provide information about the Dst index. In order to derive the Dst index, the position of the aurora must first be calculated. First the distance g between the observer and the aurora is determined by equation 7. Using equation 8 the difference between observer and aurora in longitude and latitude ($\Delta\phi$ and $\Delta\vartheta$) can be calculated. Addition of the observer position with $\Delta\phi$ and $\Delta\vartheta$ gives the position of the aurora. With the known position of the geomagnetic pole from the IGRF-12 the determined positions were converted into geomagnetic coordinates. Effects due to the changing dipole moment of the Earth's magnetic field, as discussed in *Kataoka and Kiyomi* [2017], were not included. These play a role especially over larger time scales. Furthermore, the position of the aurora at 500 km altitude was taken as reference. This position would still have to be converted with the information about inclination and declination of the local magnetic field to the foot point of the field line on the Earth's surface. Since the calculation of the Dst index is not the main focus of the present work, these steps were omitted and it was shown that even a simplified estimation gives good results. The Dst indices for the 2016 and 2017 storm were obtained from the Data Analysis Center for Geomagnetism and Space Magnetism at Kyoto University (DAC Kyoto).

For all the different methods presented in Table 1 the respective RMSD values were calculated in order to determine which auroral oval model is the preferred one.

Figure 3 shows the used sightings (red) and unused observations (blue), which were not included since some of the important information is missing. Furthermore the calculated cgm pole (red triangle) as well as the true cgm pole location (green star) is given.

3.3 Results

In this paragraph we discuss the results presented in Table 2 in more detail by looking at each geomagnetic storm individually.

3.3.1 The geomagnetic storm on March 27 and 28, 2017

On March 27 and 28, 2017 the coronal hole 798 produced a G2 geomagnetic storm with aurora activity in Europe and North America [*Möller*, 2021].

Table 2. Details of the four investigated geomagnetic storms between 2003 and 2017. Besides the date, the cause (AR - active region, CH- coronal hole), the NOAA classification as well as total number of observations and the number of sightings with all necessary information. Furthermore the maximum and average Kp indices are given together with true position of the cgm pole. The Table also contains the mean calculated parameters for the different storms.

	Halloween storm	St. Patrick's Day storm	2016 storm	2017 storm
date	Oct 29 - 30, 2003	Mar 17 - 18, 2015	May 8 - 9, 2016	Mar 27 - 28, 2017
cause	AR 486	AR 12297	CH 733	CH 798
class	G5	G4	G2	G2
total nr. obs.	207	235	104	68
nr. used obs.	128	186	78	53
Kp_{max}	9o	8–	6+	6+
$\overline{Kp}$	8+	7–	5–	5
calc. Kp index	8.2 ± 0.6	5.3 ± 1.1	4.9 ± 0.7	3.1 ± 0.9
cgm pole	82.1° N, 83.2° W	83.1° N, 84.6° W	83.2° N, 84.7° W	83.3° N, 84.9° W
calc. cgm pole	$(82.6 \pm 2.2)°$ N	$(83.7 \pm 0.4)°$ N	$(75.9 \pm 3.3)°$ N	$(82.6 \pm 2.2)°$ N
	$(95.6 \pm 7.4)°$ W	$(76.4 \pm 2.6)°$ W	$(96.5 \pm 15.4)°$ W	$(95.6 \pm 7.4)°$ W
Dst index [nT]	−400 [*Pulkkinen et al.*, 2005]	−223 [*Maurya et al.*, 2018]	−88 [*DAC Kyoto*]	−74 [*DAC Kyoto*]
calc. Dst index [nT]	−599	−269	−73	−33

We performed the methods presented in Section 2.4 and calculated the position of the cgm pole as well as the Kp index. The results for the different methods are listed in the appendix in Table A.3. In the case of the 2017 storm there was no need to limit the azimuthal interval to perform method 3 and 7.

As seen from Table A.3 the geographical latitude of the cgm pole is very similar in the different methods. Only method 4 and 8, which are based on another approach, yield different values. Nevertheless the mean calculated latitude of the cgm pole is $(82.6 \pm 2.2)°$ N and is therefore consistent with the true position. However, the deviations in the longitude are larger and vary in a range between 68.3° W and 125.1° W. The mean value of $(95.6 \pm 7.4)°$ W is within twice the confidence interval consistent with the true location. The distance between the true and the calculated pole is just (167 ± 97) km. When looking at the Kp index it is obvious that the auroral oval described by the ZP model is larger than the one described by the Holzworth model. The Kp values which were calculated by using the ZP model are smaller than the values obtained from the Holzworth model. The mean

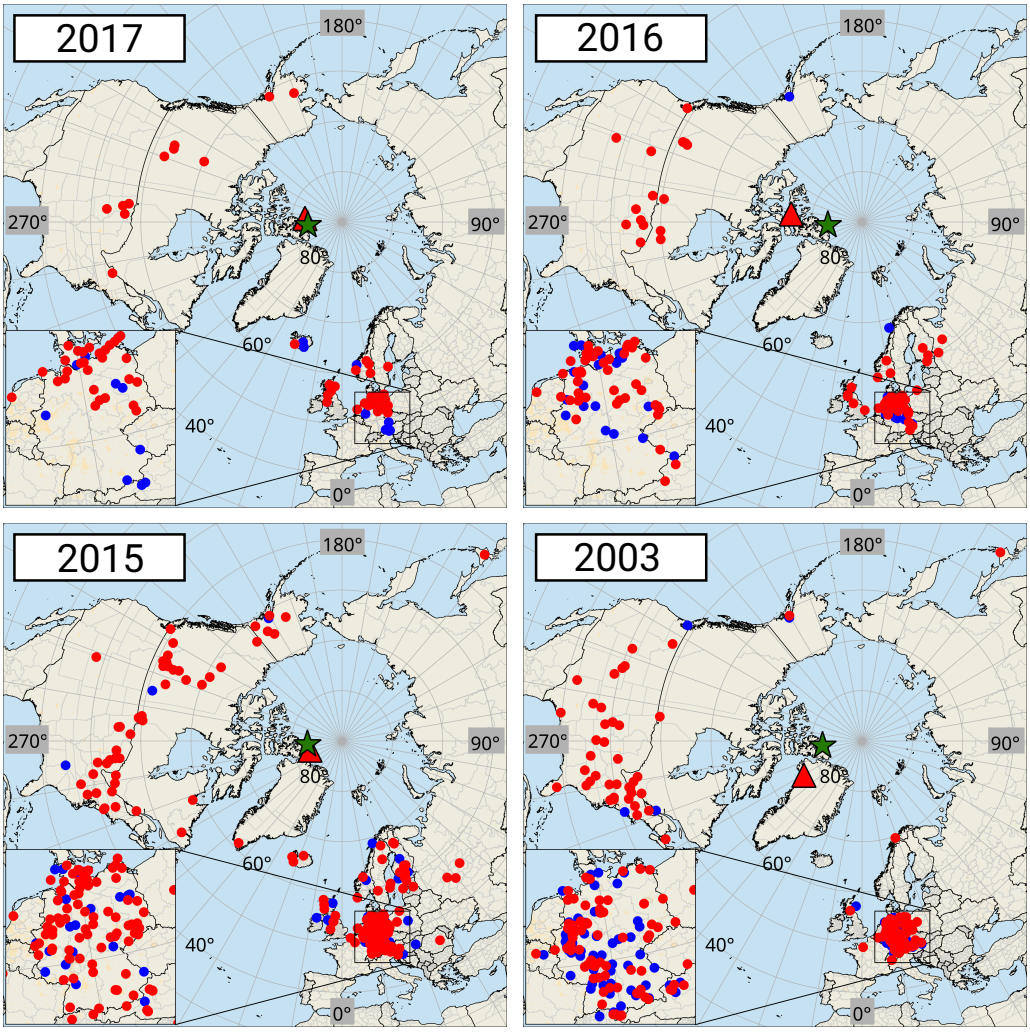

534 **Figure 3.** Distribution of the observations for the four investigated geomagnetic storms (red: used sight-
535 ings, blue: sightings which could not be used, since some required information is missing). The green star
536 shows the true position of the cgm pole according to the IGRF-12 model. The mean calculated cgm pole is
537 shown as a red triangle.

558 Kp index is 3.1 ± 0.9 which is consistent with the measured daily mean Kp index within
559 three times the confidence interval.

560 The RMSD values obtained from calculations with the Holzworth model are smaller
561 than the values from the ZP model. This indicates that in cases of a weak to medium geo-
562 magnetic storm the Holzworth model yields better results.

563 The geomagnetically equator-nearest observation was made in Webster (NY, USA)
564 with a geomagnetic latitude of 61.29° N. This results in a Dst index of −33 nT. The min-
565 imum measured Dst index, however, was −74 nT as reported by the World Data Center

for Geomagnetism in Kyoto. The discrepancy can be explained by assuming that there are observations at even lower geomagnetic latitude which were not identified so far.

3.3.2 The geomagnetic storm on May 8 and 9, 2016

The coronal hole 733 produced a G2 geomagnetic storm on May 08 and 09, 2016 with aurora activity in North America as well as Europe. Aurorae were visible by naked-eye even in the Alps [*Möller*, 2021].

The results from the different methods are shown in the appendix in Table A.4. For method 3 the azimuthal interval was restricted to [−35°,35°]. For method 7, however, where to oval is calculated in the same way as in method 3, no restriction of the azimuthal interval was necessary, since the ZP model describes a larger auroral oval. Like in the case of the 2017 storm the latitudinal positions from the different methods are consistent. Only the results obtained with approach B are different. The calculated mean latitude of $(75.9 \pm 3.3)^\circ$ N is therefore only consistent with the true position within three times the confidence interval. The longitude of the cgm is again varying in a large range between 49.8° W and 161.0° W. Nevertheless the mean calculated longitude of the pole ($(96.5 \pm 15.4)^\circ$ W) is consistent with the measured one within the confidence interval. The absolute distance between the calculated and the true cgm pole is (847 ± 272) km. The calculated mean Kp index of $\overline{\text{Kp}} = 4.9 \pm 0.7$ agrees well with the daily average of 5−.

The RMSD values for this particular storm are identical for both auroral oval models, so non of the models can be preferred in this case.

The observation in Manvel (ND, USA) was, with a geomagnetic latitude of 56.61° N, the equator-nearest observation. From this position we derived a Dst index of −73 nT, which is very close to the measured Dst index of −88 nT. Again there is a difference of 15 nT, which can be explained if there are not yet identified observations at lower geomagnetic latitudes.

3.3.3 The St. Patrick's Day storm 2015

On March 15, 2015, active region (AR) 12297 produced a fast coronal mass ejection (CME), which eventually led to a G4 geomagnetic storm, the strongest in cycle 24 [*Wang et al.*, 2016]. On March 17 (St. Patrick's Day) and March 18, 2015, strong auroral activity occurred over Europe and North America.

Table A.5 in the appendix shows the inferred positions of the cgm pole and the Kp indices based on the procedures described in Table 1. As mentioned before, the calculations with methods 3 and 7 ignore the observations for which no solution could be determined according to the respective model. In these cases, the azimuth was limited to the range $-18°$ to $18°$ and to the range $-40°$ to $40°$, leading to the omission of 37 and 9 observations, respectively. As expected, more observations are compatible with the ZP model.

It can be seen from Table A.5 that the positions of the cgm pole from all methods (except method 8) are consistent with each other. Deviations are within a few degrees. All methods have in common that they reflect the geographic latitude of the pole well, which is on average $(83.7 \pm 0.4)°$ N. The mean longitude, however, deviates by about $8°$ from the true position and is located at $(76.4 \pm 2.6)°$ W. In high latitudes, the absolute distance (see penultimate column in Table A.5) between true pole and the calculated mean cgm pole of all methods is only (124 ± 6) km. The deviations can be caused by the simplified transformation between the coordinate systems described in section 2.2. Furthermore, it is conceivable that the combination of different substorms could lead to inaccuracies. Therefore, the observations were divided into the different substorms and then the reconstruction was performed individually. After averaging the individual results, however, there was no significant improvement. This applies to the storm of 2015 as well as to the storms of 2003 discussed below. In the case of the Kp index, clear differences can be seen, meaning that the results from the calculations with the model according to *Zhang and Paxton* [2008] are significantly smaller than those from the calculations with the model according to *Holzworth et al.* [1975]. This is to be expected in the case of a moderate storm like the St. Patrick's Day storm, since the oval described by the ZP model is significantly larger than the oval from the Holzworth model. On average, however, the Kp index is $\overline{\mathrm{Kp}} = 5.3 \pm 1.1$ and is within less than 1.5 times the confidence interval consistent with daily average of $\overline{\mathrm{Kp}} \approx 7-$ (Kp = 6.67).

When looking at the RMSD values, it is noticeable that the results obtained with approach A are in the same range (RMSD $\sim$ 23). In contrast to the calculation from synthetic observations, there are no significant deviations from methods 1 and 5. In the case of methods 4 and 8, the auroral position is used for the calculation. The conversion into Cartesian coordinates results in clearly different values here, so that these two methods are only comparable with each other. The RMSD values show no clear differences between

the two oval models. Therefore, neither of the two models can be classified as more probable at this point.

The geomagnetically equator-nearest observation for the St. Patrick's Day storm was made with a geomagnetic latitude of 46.78° N in Hokkaido (JPN). By means of equation 10 this results in a minimum Dst index of −269 nT. This is very close to the measured value of Dst = −223 nT from *Maurya et al.* [2018].

3.3.4 The Halloween storm 2003

At the end of October 2003 in solar cycle 23 AR 486 produced a series of strong eruptions. With a size of about 13 Earth radii, AR 486 was the largest observed active region since 1990. On October 28, 2003, AR 486 was near the center of the solar disk and produced an X17 eruption at 11:10 UT followed by the fourth strongest CME since measurements began in 1976. This CME reached the Earth on October 29, 2003 at 06:13 UT and caused a violent G5 geomagnetic storm, accompanied by extremely high auroral activity. This was the sixth strongest geomagnetic storm since 1932 [*Balch et al.*, 2004].

The results in the appendix Table A.6 show larger deviations than for the 2015 storm. In the case of method 3 and 7 observations were neglected due to the limited azimuth interval. This concerns 49 observations in the third method ($-33° \leq \overline{az} \leq 33°$) and 47 observations in method 7 ($-35° \leq \overline{az} \leq 35°$). The calculated latitude of the cgm pole is on average $(76.2 \pm 2.5)°$ N and thus deviates from the true latitude by about 6°. Within 3 times the confidence interval, however, the values are consistent with each other. For the longitude, with an average of $(59.9 \pm 7.5)°$ W, the average deviation is much greater at about 23°. Here both values are not consistent within 3 times the confidence interval. This results in an absolute distance of the true pole to the calculated cgm pole of (810 ± 336) km. The mean calculated Kp index is $\overline{\mathrm{Kp}} = 4.2 \pm 0.6$ and is therefore not consistent with the measured daily mean of 8+. The RMSD values show a similar picture as for the St. Patrick's Day storm in 2015. Again, using approach A, the RMSD values are in a similar range of magnitude, with the values for the 2003 storm being higher than for the 2015 storm. This is consistent with the greater deviation between the calculated and true cgm pole. Again, neither of the two models can be preferred on the basis of the RMSD. The difference between the St. Patrick's Day and the Halloween storm lies in the availability and quality of the data. The few photographs of the Halloween storm are of much worse quality, so that in several cases it was not possible to determine the position

of the aurora. In addition, in many cases only written reports were available which are less accurate in providing the required data compared to photographs.

The latitude for the Halloween storm remains consistent only within 3 times the confidence interval. Deviations in the position of the pole therefore also lead to inaccuracies in the Kp index. The calculated cgm pole is shifted to lower latitudes. Therefore a smaller oval is consistent with the aurora sightings which leads to a decreased Kp index. Hence, if the data is insufficient or the number of observations is small, a simplification of the program should be considered in the sense that the position of the pole is given and only the Kp index is calculated. By specifying the above mentioned position of the cgm pole from IGRF-12, this leads to a mean Kp index for the 2003 storm of 8.2 ± 0.6, which corresponds very well with the measured mean Kp index of 8+.

During this storm the geomagnetically equator-nearest auroral position is at a latitude of 38.54° N and belongs to an observation from Orlando in Florida (USA). This results in a Dst index of −599 nT. After *Pulkkinen et al.* [2005] the lowest Dst-index is −400 nT, which in this case differs quite strongly from the value calculated here. The reason for this are the simplifications in the estimation of the Dst index listed in section 3.2, why the Dst index presented here is a lower limit. This is consistent with the findings in *Hayakawa et al.* [2018].

4 Conclusion

We reconstructed the auroral oval from ground-based observations using Bayesian inference, which allows statements about the position of the pole in cgm coordinates as well as the magnetic activity of the terrestrial field described by the Kp index. Two models of the auroral oval were used for this purpose, the one by *Holzworth et al.* [1975] and a somewhat larger oval described by *Zhang and Paxton* [2008]. With these models it is possible to calculate a theoretical elevation angle of the aurora for each observation. The obtained theoretical value is then compared with the elevation angle derived from reports or photographs.

To test the method, artificial observations were created for which the position of the cgm pole and the Kp index are known. It could be shown that the different methods could determine the given parameters for observations with an nonuniform longitudinal distribution mimicking real observations. Even after a random variation of the observed auroral

elevation angle within a 10° interval the given values could be determined. The differences between the calculations with and without variations are negligible.

On the basis of synthetic observations as well as the St. Patrick's Day storm, the 2016 and 2017 geomagnetic storm, it could be shown that the method developed in this paper can precisely calculate the position of the cgm pole and the Kp index for good data quality, with a deviation in longitude already occurring in the case of the 2015, 2016 and 2017 storm ($\sim 10°$). If the data are less accurate, i.e. if the position of the aurora is less well determined, larger deviations occur especially in the longitude of the pole. This is seen in the Halloween storm 2003 where larger longitudinal deviations occur. There are several reasons for this behaviour.

The auroral oval models from *Holzworth et al.* [1975] and *Zhang and Paxton* [2008] are empirical models. Since strong and extreme storms occur significantly less frequently, the models are less accurate, especially for those cases. Further inaccuracies result from the simplified coordinate transformation between cgm and geographic coordinate system as presented in *Sigernes et al.* [2011]. Furthermore, inaccuracies could be caused by the merging of different substorms, which could be excluded. On the other hand, both oval models, due to the underestimated oval extension, do not provide results for some observations, so that these observations must either be neglected or the assumption must be made that these observations were made in magnetic north direction. Another possibility to circumvent this problem is to calculate the auroral position in 3D Cartesian coordinates from the information given in the reports or obtained from the photographs. This can then be compared with the nearest oval position. This approach provides a solution for all observations. However, a manipulation of the data in the form of the calculation of the aurora position is necessary. Derived quantities from observations are usually not desired in Bayesian inference as they possess reshaped error distributions which need to be tracked carefully. If, as before, the theoretical aurora position is compared with the true elevation angle of the aurora, the information from the reports can be used directly.

On average we found a difference between the true and calculated cgm pole location of $(2.3 \pm 1.7)°$ in latitude and $(10.8 \pm 0.9)°$ in longitude. For the Kp index the derived values are off by around 0.9 ± 0.4, if the corrected value for the 2003 storm is used, and 1.7 ± 0.7, if the uncorrected value is taken into account. This indicates, that the method is capable of determining the latitude of the cgm pole very accurate, but on average there is a discrepancy in longitude of around 10°, which arises most likely from missing East

Asian observation in case of the 2016 and 2017 storm and from an underestimation of the auroral oval in both models in case of the strong 2003 Halloween storm. The Kp index can be obtained with an accuracy of around ± 1.

The RMSD was calculated for all methods to see how well the resulting auroral oval fits the data. The RMSD values are similar for both auroral models, meaning that non of both models can be preferred. Furthermore the RSMD values are comparable to the assumed standard deviation of the likelihood, indicating that our uncertainties are neither over- nor underestimated.

The next step is to apply the presented method to storms before 1900 to determine Kp and Dst indices and possibly also the location of the cgm pole. The aurora catalogue from *Fritz* [1873] lists 46 geomagnetic storms with a sufficient number of observations during the last 400 years. We will show in a following article, that there is large number of observations for those historical storms, where the original reports are available and can be analysed in order to derive the required information. For example, we have identified 532 observations for the Carrington event in 1859, with 168 observation containing the necessary information. The obtained data can first be used for comparison with the position of the geomagnetic pole from different paleomagnetic field models. Secondly, the calculated Kp index can help to study past solar activity, since the magnetic activity of the terrestrial field is linked to solar activity.

A: Appendix

Table A.1. Results of the calculations based on synthetic observations using the Holzworth model (white rows) and the ZP model (grey rows). The upper half shows the results of all 40 generated observations. The lower half was obtained without the East Asian observations. The original position of the cgm pole was 83.1° N and 84.0° W, the Kp index was 6.

nr.	approach	geo. latitude [°]	geo. longitude [°]	Kp index	distance [km]	RMSD
1	A	82.8 ± 0.1	−88.6 ± 3.8	5.3 ± 0.5	71 ± 35	4.21°
2	A	83.1 ± 0.1	−84.1 ± 3.5	6.0 ± 0.4	1 ± 1	2.58°
3	A	83.1 ± 0.1	−84.2 ± 4.0	6.0 ± 0.5	3 ± 2	2.14°
4	B	83.6 ± 0.1	−86.9 ± 9.2	5.7 ± 1.0	67 ± 38	350 km
5	A	82.9 ± 0.1	−89.0 ± 1.7	5.9 ± 0.1	71 ± 17	4.64°
6	A	83.2 ± 0.1	−85.1 ± 2.2	5.9 ± 0.1	18 ± 17	2.21°
7	A	83.0 ± 0.1	−84.2 ± 1.7	6.0 ± 0.1	11 ± 2	0.73°
8	B	83.5 ± 0.1	−86.7 ± 9.1	5.9 ± 0.3	57 ± 36	270 km
nr.	**approach**	**geo. latitude [°]**	**geo. longitude [°]**	**Kp index**	**distance [km]**	**RMSD**
1	A	82.9 ± 0.1	−88.9 ± 4.0	5.4 ± 0.6	70 ± 42	4.26°
2	A	83.1 ± 0.1	−84.2 ± 3.6	6.0 ± 0.5	3 ± 2	2.68°
3	A	83.1 ± 0.1	−84.4 ± 4.1	6.0 ± 0.6	5 ± 5	2.17°
4	B	83.9 ± 0.2	−91.9 ± 13.8	6.2 ± 1.4	133 ± 94	360 km
5	A	84.1 ± 0.1	−92.5 ± 5.0	6.4 ± 0.3	153 ± 48	4.71°
6	A	83.1 ± 0.1	−84.3 ± 4.0	6.1 ± 1.7	4 ± 4	2.98°
7	A	83.1 ± 0.1	−84.4 ± 4.1	6.0 ± 1.9	5 ± 5	1.83°
8	B	83.9 ± 0.2	−93.6 ± 15.0	6.1 ± 0.5	150 ± 113	290 km

749 **Table A.2.** Results of the calculations based on synthetic observations. The calculations using the Holz-
750 worth model are highlighted in white, while the lines with a grey background show the results using the ZP
751 model. The upper table shows the results of all 40 generated observations. The lower table contains the results
752 obtained when the East Asian observations are neglected. The given position of the CGM pole is 83.1° N and
753 84.0° W, where a Kp index of 6 was chosen.

nr.	approach	geo. latitude [°]	geo. longitude [°]	Kp index	distance [km]	RMSD
1	A	82.9 ± 0.1	−87.5 ± 3.8	5.3 ± 0.5	52 ± 33	4.25°
2	A	83.2 ± 0.1	−82.9 ± 3.3	6.0 ± 0.4	18 ± 11	3.17°
3	A	83.2 ± 0.1	−83.0 ± 3.7	6.1 ± 0.5	17 ± 11	3.08°
4	B	83.4 ± 0.1	−87.7 ± 9.1	5.0 ± 0.9	59 ± 51	370 km
5	A	82.9 ± 0.1	−89.0 ± 1.7	5.9 ± 0.1	71 ± 17	5.50°
6	A	83.1 ± 0.1	−84.6 ± 2.2	5.9 ± 0.1	8 ± 7	3.34°
7	A	82.9 ± 0.1	−83.7 ± 3.0	6.0 ± 0.1	23 ± 9	3.12°
8	B	83.5 ± 0.1	−86.6 ± 9.1	5.9 ± 0.3	56 ± 38	290 km

nr.	approach	geo. latitude [°]	geo. longitude [°]	Kp index	distance [km]	RMSD
1	A	83.0 ± 0.1	−87.7 ± 3.8	5.4 ± 0.5	51 ± 39	5.24°
2	A	83.2 ± 0.1	−83.1 ± 3.5	6.0 ± 0.5	16 ± 9	3.03°
3	A	83.2 ± 0.1	−83.3 ± 3.8	6.1 ± 0.6	15 ± 7	2.87°
4	B	83.3 ± 0.3	−98.0 ± 27.5	5.9 ± 2.0	185 ± 172	390 km
5	A	84.0 ± 0.1	−91.7 ± 4.3	6.3 ± 0.3	139 ± 43	5.26°
6	A	83.4 ± 0.1	−86.5 ± 4.1	6.0 ± 0.2	47 ± 33	3.27°
7	A	82.7 ± 0.1	−83.9 ± 6.2	6.0 ± 0.2	45 ± 7	3.66°
8	B	83.6 ± 0.2	−91.2 ± 14.7	6.0 ± 0.5	108 ± 92	300 km

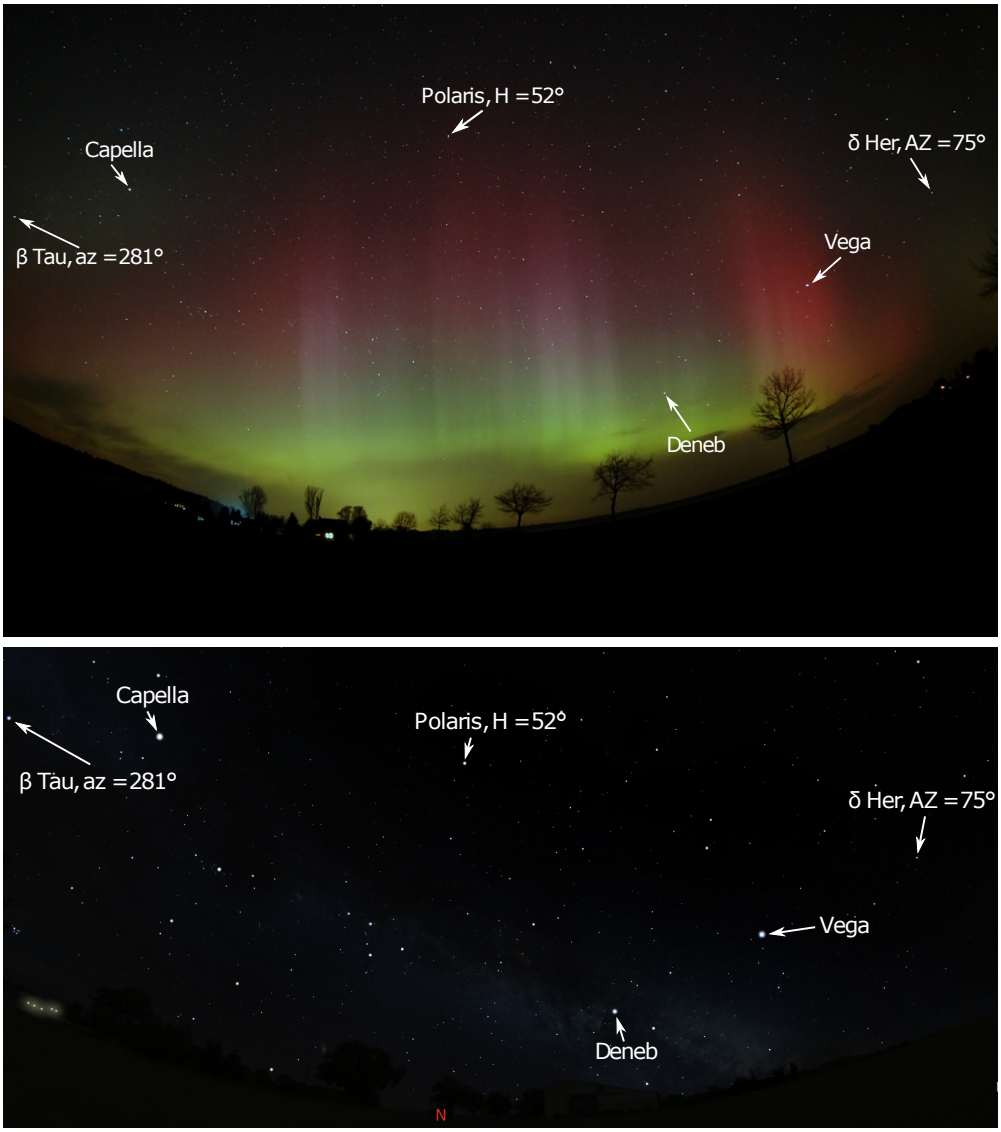

754 **Figure A.1.** Top panel: Photograph of the Aurora Borealis in Hartenholm (courtesy of Hartwig Lüthen)
755 on March 17, 2015 at 23:30 LT. The positions of bright stars were used to estimate the elevation angle and
756 azimuth of the aurora in the sky by using *Stellarium* (bottom panel)).

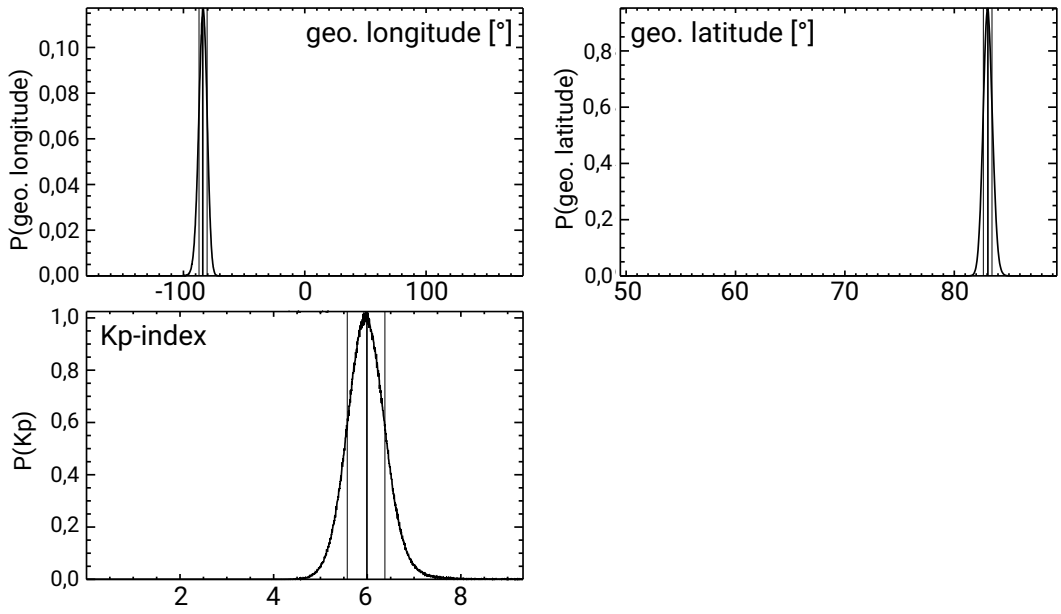

Figure A.2. Results of method 2 for the longitude and latitude of the cgm pole and the Kp index. Clear peaks in the probability distribution of all parameters can be identified. The thin lines denote the confidence intervals of the parameters, while the thick line is the average parameter value. The given values were reproduced.

Table A.3. Results of the geomagnetic storm in 2017. All results are given together with the 68 % confidence intervals. The penultimate column describes the distance between the calculated and true position of the cgm pole in km, with the last column indicating the RMSD. The methods using the ZP model are marked in gray. The last row contains the mean position of the cgm pole from all calculations and the mean Kp index together with the 1 σ standard errors. The distance given here is the distance between the mean calculated pole from aurorae and true cgm pole at 83.3° N and 84.9° W. The measured daily mean Kp index was 5.

nr.	approach	geo. latitude [°]	geo. longitude [°]	Kp index	distance [km]	RMSD
1	A	88.7 ± 0.6	-85.4 ± 1.8	4.9 ± 0.3	603 ± 63	20.05°
2	A	88.8 ± 0.5	-99.6 ± 7.2	2.9 ± 0.5	620 ± 58	16.68°
3	A	82.3 ± 0.1	-100.7 ± 5.8	3.0 ± 0.4	213 ± 71	11.81°
4	B	71.3 ± 1.3	-68.3 ± 7.7	2.4 ± 1.0	1381 ± 186	871 km
5	A	86.1 ± 0.4	-83.3 ± 32.1	8.3 ± 0.6	310 ± 9	26.58°
6	A	83.7 ± 0.1	-124.9 ± 25.1	1.3 ± 0.7	496 ± 290	14.87°
7	A	83.8 ± 0.1	-125.1 ± 25.1	1.3 ± 0.7	498 ± 289	14.87°
8	B	75.2 ± 1.1	-77.7 ± 17.8	0.3 ± 0.3	910 ± 171	725 km
		82.6 ± 2.2	-95.6 ± 7.4	3.1 ± 0.9	167 ± 97	

768 **Table A.4. Results of the geomagnetic storm in 2016. All results are given together with the 68 %**
769 **confidence intervals. The penultimate column describes the distance between the calculated and true**
770 **position of the cgm pole in km, with the last column indicating the RMSD. The methods using the ZP**
771 **model are marked in gray. The last row contains the mean position of the cgm pole from all calcu-**
772 **lations and the mean Kp index together with the 1 σ standard errors. The distance given here is the**
773 **distance between the mean calculated pole from aurorae and true cgm pole at 83.2° N and 84.7° W. The**
774 **measured daily mean Kp index was 5−.**

nr.	approach	geo. latitude [°]	geo. longitude [°]	Kp index	distance [km]	RMSD
1	A	81.7 ± 0.1	-93.7 ± 6.6	4.5 ± 0.6	210 ± 46	16.73°
2	A	81.8 ± 0.1	-90.5 ± 5.4	4.6 ± 0.5	174 ± 25	15.27°
3	A	82.4 ± 0.1	-96.2 ± 9.6	5.2 ± 1.1	185 ± 97	15.67°
4	B	60.4 ± 1.3	-49.8 ± 2.9	6.9 ± 1.6	2701 ± 165	1168 km
5	A	69.1 ± 4.2	-65.5 ± 26.7	8.0 ± 0.7	1624 ± 610	28.01°
6	A	82.8 ± 0.1	-160.9 ± 7.1	4.7 ± 0.4	961 ± 72	15.78°
7	A	82.8 ± 0.1	-161.0 ± 7.1	4.7 ± 0.4	962 ± 71	15.78°
8	B	65.8 ± 2.2	-54.2 ± 7.7	0.9 ± 0.7	2080 ± 306	1022 km
		75.9 ± 3.3	-96.5 ± 15.4	4.9 ± 0.7	847 ± 272	

775 **Table A.5.** Results of the St. Patrick's Day storm in 2015. All results are given together with the 68 % con-
776 fidence intervals. The penultimate column describes the distance between the calculated and true position of
777 the cgm pole in km, with the last column indicating the RMSD. The methods using the ZP model are marked
778 in gray. The last row contains the mean position of the cgm pole from all calculations and the mean Kp index
779 together with the 1 σ standard errors. The distance given here is the distance between the mean calculated
780 pole from aurorae and true cgm pole at 83.1° N and 84.6° W. The measured daily mean Kp index was 7−.

nr.	approach	geo. latitude [°]	geo. longitude [°]	Kp index	distance [km]	RMSD
1	A	82.4 ± 0.1	-72.9 ± 2.0	7.0 ± 0.6	181 ± 30	22.90°
2	A	84.3 ± 0.1	-76.6 ± 1.7	8.5 ± 0.6	165 ± 8	23.54°
3	A	83.5 ± 0.1	-73.3 ± 2.1	8.1 ± 0.7	152 ± 25	26.03°
4	B	83.3 ± 0.1	-73.1 ± 4.0	8.3 ± 0.7	159 ± 10	550 km
5	A	82.8 ± 0.1	-73.3 ± 2.2	2.3 ± 0.1	161 ± 13	22.94°
6	A	83.2 ± 0.1	-73.5 ± 2.8	2.5 ± 0.1	148 ± 37	22.86°
7	A	84.1 ± 0.1	-75.5 ± 3.1	2.6 ± 0.1	153 ± 11	23.39°
8	B	85.9 ± 0.1	-92.9 ± 17.4	3.2 ± 0.5	324 ± 50	490 km
		83.7 ± 0.4	-76.4 ± 2.6	5.3 ± 1.1	124 ± 6	

781 **Table A.6.** Results of the 2003 Halloween storm. All results are given together with the 68 % confidence
782 intervals. The penultimate column describes the distance between the calculated and true position of the cgm
783 pole in km, with the last column indicating the RMSD. The methods using the ZP model are marked in gray.
784 The penultimate row contains the mean position of the cgm pole from all calculations and the mean Kp index
785 together with the 1 σ standard errors. The distance given here is the distance between the mean calculated
786 pole from aurorae and true cgm pole at 82.1° N and 83.2° W. The last rows shows the mean calculated Kp
787 index with the cgm pole position fixed at the true value. The measured daily mean Kp index was 8+.

nr.	approach	geo. latitude [°]	geo. longitude [°]	Kp index	distance [km]	RMSD
1	A	74.3 ± 0.2	-51.3 ± 1.2	4.6 ± 0.3	1104 ± 35	23.49°
2	A	76.0 ± 0.2	-49.2 ± 1.4	4.8 ± 0.3	964 ± 38	24.24°
3	A	78.9 ± 0.2	-53.7 ± 1.3	6.4 ± 0.4	640 ± 35	27.92°
4	B	69.9 ± 0.8	-47.0 ± 3.5	4.8 ± 1.1	1614 ± 128	100 km
5	A	79.6 ± 0.1	-60.0 ± 1.6	2.9 ± 0.2	487 ± 32	22.96°
6	A	84.0 ± 0.1	-78.7 ± 2.6	4.7 ± 0.2	218 ± 4	23.81°
7	A	81.2 ± 0.1	-96.3 ± 3.5	4.2 ± 0.3	235 ± 44	30.23°
8	B	65.6 ± 0.9	-42.9 ± 4.2	1.4 ± 0.5	2122 ± 149	110 km
		76.2 ± 2.5	-59.9 ± 7.5	4.2 ± 0.6	810 ± 336	
		fixed	fixed	8.2 ± 0.6		

788 ## Acknowledgments

789 We acknowledge useful discussion with Monika Korte, Hans-Erich Fröhlich and Va-
790 leri Hambaryan. Furthermore we thank Hartwig Lüthen for providing his aurora photo-
791 graph taken in Hartenholm on March 17, 2015.

792 This publication makes use of the Kp and Dst index database operated by the Data
793 Analysis Center for Geomagnetism and Space Magnetism at Kyoto University (`http:`
794 `//wdc.kugi.kyoto-u.ac.jp/kp/index.html`). Most of the aurora reports and images
795 were obtained from the aurora archives from Andreas Möller (`http://www.polarlicht-archiv.`
796 `de/`) and Aurorasaurus (`https://www.aurorasaurus.org/`) [*MacDonald et al.*, 2015].

References

Akasofu, S.-I. (2009). The Northern Lights: Secrets of the Aurora Borealis. *Alaska Northwest Books*

D'Agostini, G. (2003). Bayesian inference in processing experimental data: principles and basic applications. *Reports on Progress in Physics*, Volume 66, Issue 9, pp. 1383–1419.

Arlt, R., Leussu, R., Giese, N., Mursula, K., Usoskin, I.G. (2013). Sunspot positions and sizes for 1825 - 1867 from the observations by Samuel Heinrich Schwabe. *Mon. Not. R. Astron. Soc.*, 433, 3165–3172.

Balch, C., Crown, M.D., Viereck, R. (2004). Overview of Space Weather, Space Weather Forecasts, and System Impacts During the High Activity from 19 October through 7 November 2003. *American Astronomical Society Meeting 204, Bulletin of the American Astronomical Society*, Volume 36, p. 670.

Bartels, J., Heck, N.H., Johnston, H.F. (1939). The three-hour-range index measuring geomagnetic activity. *Terrestrial Magnetism and Atmospheric Electricity*, Volume 44, Issue 4, p. 411.

Bayes, T. (1764). An Essay Toward Solving a Problem in the Doctrine of Chances. *Philosophical Transactions of the Royal Society of London*, Volume 53, pp. 370–418.

Bekli, M.R., Chdaou, I. (2019). Analysis of pre-telescopic sunspots and auroras from 8th to 16th century. *Advances in Space Research*, Volume 46, Issue 4, pp. 1011–1018

Boteler, D.H. (2019). A 21st Century View of the March 1989 Magnetic Storm. *Space Weather*, Volume 17, Issue 10, pp. 1427–1441.

Campbell, E.P. (2004). An introduction to physical-statistical modelling using Bayesian methods. *CSIRO Mathematical und Information Sciences*, `http://www.ioci.org.au/publications/cat_view/16-ioci-stage-2/34-technical-papers.html`, accessed: 19.01.2020.

Clette, F., Svalgaard, L., Vaquero, J.M., Cliver, E.W. (2014). Revisiting the Sunspot Number. *Solar and Stellar Astrophysics*, Volume 186, p. 35–103.

Corsaro, E., Fröhlich, H. -E., Bonanno, A., Huber, D., Bedding, T. R., Benomar, O., De Ridder, J., Stello, D. (2013). A Bayesian approach to scaling relations for amplitudes of solar-like oscillations in Kepler stars. *Monthly Notices of the Royal Astronomical Society*, Volume 430, Issue 3, pp. 2313–2326.

Delaygue, G., Bard, E. (2011). An Antarctic view of Beryllium-10 and solar activity for the past millennium. *Climate Dynamics*, Volume 36, No. 11, p. 2201–2218.

Department of Defense (1991). World Geodetic System 1984. Its definition and relationships with local geodetic systems. *US Government, Department of Defense, Rockville, MD, 1991*.

Emmert, J.T., Richmond, A.D., Drob, D.P. (2010). A computationally compact representation of Magnetic-Apex and Quasi-Dipole coordinates with smooth base vectors. *J. Geophys. Res.*, 115 (A8).

Feldstein, Y.I. (1964). Auroral morphology, I. The location of the auroral zone. *Tellus*, Volume 16, Issue 2, p.252.

Fritz, H. (1873). Verzeichnis beobachteter Polarlichter. C. Gerold's Sohn (Wien)

Fröhlich, H. -E., Frasca, A., Catanzaro, G., Bonanno, A., Corsaro, E., Molenda-Żakowicz, J., Klutsch, A., Montes, D. (2012). Magnetic activity and differential rotation in the young Sun-like stars KIC 7985370 and KIC 7765135. *Astronomy and Astrophysics*, Volume 543, A146.

Hastings, W.K. (1970). Monte Carlo Sampling Methods Using Markov Chains and Their Applications. *Biometrika*, Volumne 57, pp. 97-âĂŞ109.

Hayakawa, H., Ebihara, Y., Willis, D.M., Hattori, K., Giunta, A.S., Wild, M.N., Hayakawa, S., Toriumi, S., Mitsuma, Y., Macdonald, L.T., Shibata, K., Silverman, S.M. (2018). The Great Space Weather Event during 1872 February Recorded in East Asia. *The Astrophysical Journal*, Volume 862, Issue 1.

Holzworth, R.H., Meng, C.I. (1975). Mathematical representation of the Auroral Oval. *Geophysical Research Letters*, Vol. 2, No. 9.

Kataoka, R., Kiyomi, I. (2017). Inclined Zenith Aurora over Kyoto on 17 September 1770: Graphical Evidence of Extreme Magnetic Storm. *Space Weather,* Volume 15, Issue 10, pp. 1314–1320.

Korte, M., Stolze, S. (2016). Variations in Mid-Latitude auroral activity during the Holocene. *Archaeometry* 58, 1, 159–176.

Korte, M., Brown, M., Frank, U., Senftleben, R., Nowaczyk, N. (2018). Global Geomagnetic Field Reconstructions from Centuries to Excursions. *Magnetic Fields in the Solar System. Series: Astrophysics and Space Science Library*, Volume 448, pp. 83–110.

Kosar, B.C., MacDonald, E.A., Case, N.A., Zhang, Y., Mitchell, E.J., Viereck, R. (2018). A case study comparing citizen science aurora data with global auroral boundaries de-

rived from satellite imagery and empirical models. *Journal of Atmospheric and Solar-Terrestrial Physics*, Volume 177, p. 274–282.

Laundal, K.M., Richmond, A.D. (2017). Magnetic Coordinate Systems. *Space Science Reviews*, Volume 206, Issue 1–4, pp. 27–59.

MacDonald, E.A., Case, N.A., Clayton, J.H., Hall, M.K., Heavner, M., Lalone, N., Patel, K.G., Tapia, A. (2015). Aurorasaurus: A citizen science platform for viewing and reporting the aurora. *Space Weather*, Volume 13, Issue 9, pp. 548–559.

Maurya, A.K., Venkatesham, K., Kumar, S., Singh, R., Tiwari, P., Singh, A.K. (2018). Effects of St. Patrick's Day Geomagnetic Storm of March 2015 and of June 2015 on Low-Equatorial D Region Ionosphere. *J. Geophys. Res.*, Volume 123, Issue 8, pp. 6836–6850.

Möller, Andreas (2013–2021). Polarlicht-Archiv. `http://www.polarlicht-archiv.de/`, accessed: 19.01.2021.

Neuhäuser, R., Neuhäuser, D.L. (2015a). Solar activity around AD 775 from aurorae and radiocarbon. *Astronomical Notes*, 336, 225–248.

Neuhäuser, R., Neuhäuser, D.L. (2015b). Variations of 14-C around AD 775 and AD 1795 - due to solar activity. *Astronomical Notes*, 336, 930–954.

Newell, P.T., Sotirelis, T., Wing, S. (2009). Diffuse, monoenergetic, and broadband aurora: The global precipitation budget. *J. Geophys. Res.*, Volume 114, Issue A9.

Pesnall, W.D. (2016). Watching the Sun from space. *Asian Journal of Physics*, Volume 25, No. 3, 233–265.

Pulkkinen, A., Lindahl, S., Viljanen, A., Pirjola, R. (2005). Geomagnetic storm of 29âĂŞ31 October 2003: Geomagnetically induced currents and their relation to problems in the Swedish high-voltage power transmission system. *Space Weather*, Volume 3, Issue 8.

Robert, C.P. (2016). The Metropolis-Hastings algorithm. *arXiv:1504.01896v3*.

Sabine, E. (1852). On periodical laws discoverable in the mean effects of the larger magnetic disturbance. *Philos. Trans.*, 142, 103–124.

Sigernes, F., Dyrland, M., Brekke, P., Gjengedal, E.K., Chernouss, S., Lorentzen, D.A., Oksavik, K., Deehr, C.S. (2011). Real time aurora oval forecasting - SvalTrackII. *Optica Pura y Aplicada (OPA)*, Volume 44, Issue 4, pp. 599–603.

Sigernes, F., Dyrland, M., Brekke, P., Chernouss, S., Lorentzen, D.A., Oksavik, K., Deehr, C.S. (2011). Two methods to forecast auroral displays. *J. Space Weather Space Clim.*, 1,

A03.

Siscoe, G.L., Verosub, K.L. (1983). High medieval auroral incidence over China and Japan: Implications for the medieval site of the geomagnetic pole. *Geophysical Research Letters*, Volume 10, Issue 4, pp. 345–348.

Starkov, G.V. (1994). Mathematical model of the auroral boundaries. *Geomagnetism and Aeronomy*, Volume 34, Issue 2.

Thebault, E. et al. (2015). International Geomagnetic Reference Field: the 12th generation. *Earth, Planets and Space*, 67:79

Usoskin, I.G. (2017). A history of solar activity over millennia. *Living Reviews in Solar Physics*, Volume 14, Issue 1.

Wagner, D., Neuhäuser, R. (2019). Variation of the auroral oval size and offset for different magnetic activity levels described by the Kp-index. *Astronomical Notes*, 2019;1–11.

Wagner, D. (2020). Rekonstruktion des Polarlichtovals anhand bodengebundener Beobachtungen. *Friedrich-Schiller-Universität Jena*

Wang, Y. et al. (2016). On the Propagation of a Geoeffective Coronal Mass Ejection during March 15-17, 2015. *:1607.07750*

Yokoyama, N., Kamida, Y., Miyaoka, H. (1998). The size of the auroral belt during magnetic storms. *Ann. Geophys.*, 16, 566–573.

Zhang,Y., Paxton, L.J. (2008). An empirical Kp-dependent global auroral model based on TIMED/GUVI FUV data. *Journal of Atmospheric and Solar-Terrestrial Physics*, 70, 1231–1242.

Zotti, G., Wolf, A., Gates, M., Gerde, B. (2017). Stellarium 0.16.1 User Guide. `https://www.researchgate.net/publication/319987634_Stellarium_0161_User_Guide`, accessed: 11.02.2018.